The range-resident logistic model: a new framework to formalize the population-dynamics consequences of range residency

Rafael Menezes[1,2], Justin M. Calabrese[2,3,4], William F. Fagan[4], Paulo Inácio Prado[1], and Ricardo Martinez-Garcia[2,5,*]

[1]Universidade de São Paulo, Brazil
[2]Center for Advanced Systems Understanding (CASUS), Helmholtz-Zentrum Dresden-Rossendorf (HZDR), Görlitz, Germany
[3]Department of Ecological Modelling, Helmholtz Centre for Environmental Research – UFZ, Leipzig, Germany
[4]Department of Biology, University of Maryland, College Park, MD, USA
[5]ICTP South American Institute for Fundamental Research and Instituto de Física Teórica, Universidade Estadual Paulista - UNESP, São Paulo, Brazil
[*]Corresponding author: r.martinez-garcia@hzdr.de

February 10, 2025

Keywords: Movement ecology, Population dynamics, Range residency, Spatial modeling, Individual-based modeling

Abstract

Individual movement is critical in shaping population dynamics. However, theoretical frameworks linking these two processes often make unrealistic assumptions about how animals move or, when attempting to incorporate realistic movement patterns, must rely on numerical simulations. To address this gap, we introduce the range-resident logistic model, which is an easy-to-simulate and mathematically tractable extension of the spatial logistic model that incorporates empirically supported range-resident movement. Our framework unifies previous non-spatial and (sessile) spatial formulations of the logistic model as limiting cases, recovering these two limits when home ranges are infinitely large and vanishingly small, respectively. Interpolating between these two regimes, the long-term population size depends nonlinearly on home-range size and spatial distribution. Neglecting range residency can hence lead to significantly under- or overestimating population carrying capacity. To better understand these results, we also

introduce a novel crowding index that depends on movement parameters and can be estimated from tracking data. This index captures the influence of spatial structure on population size, and serves as a robust predictor of abundance. The range-resident logistic model is thus a unifying framework bridging movement and population ecology, and provides new insights into how different patterns of individual space usage shape intraspecific interactions and regulate population growth.

1 Introduction

Recent advances in tracking technology, data-sharing platforms, and statistical analyses have provided unprecedented insight into how organisms move, including a more precise quantification of their home ranges [1–5]. Home ranges, which encapsulate the areas that animals regularly use for securing resources and caring for offspring, are ubiquitous across animal species [6]. Home-range size and overlap determine how often organisms encounter one another, which makes them key drivers of intra and interspecific interactions [7–10]. However, although we can accurately estimate home-range sizes as well as encounters and their consequences for range-resident animals, we still do not fully understand their quantitative impact on population and community dynamics [10–18]. Establishing a theoretical link between range-resident movement and population dynamics is critical to answering many applied questions in population and community ecology [19, 20].

Theoretical ecology has mainly developed from non-spatial models that only track abundances and assume homogeneously distributed populations where organisms interact via the law of mass action [21–23]. This approach oversimplifies movement, and neglects the influence of within-range movement upon population dynamics. Spatially explicit approaches, such as metapopulation models or reaction-diffusion equations, incorporate different movement and dispersal modes [24, 25]. However, they still assume well-mixed conditions at the scale of interactions. Finally, individual-based models (IBM) can describe movement at almost any level of detail, including range residency, and are easy to parameterize for specific populations [26]. Computational simulations of IBMs with range-resident movement have helped us understand the causes of territoriality [27], and how environmental and intraspecific trait variability promote the stability of animal communities [28–30].

Therefore, IBMs have revealed some of the mechanisms underlying home-range spatial dynamics and are more straightforwardly transferred to conservation and management. Yet, with current analytical tools, IBMs are mathematically tractable only for Brownian movement—which does not describe range residency and converges to well-mixed conditions if organisms explore the entire available environment between demographic processes—or sessile organisms [31–33]. This lack of mathematical tractability and their system-specific nature make most IBMs an inappropriate basis from which to extract general conclusions on how movement parameters affect population dynamics.

A promising direction lies in identifying alternative stochastic processes that can simultaneously maintain analytical tractability while improving the realism of simulated animal movement. The Ornstein-Uhlenbeck (OU) stochastic process is an optimal compromise, as it correctly captures the main two features of range residency: home ranges covering only a fraction of the total population range and non-uniform utilization of each home-range area. Additionally, a recent multispecies comparative study of home ranges based on GPS tracking data identified OU process and its variant incorporating autocorrelated velocities—the Ornstein-Uhlenbeck with Foraging (OUF) process—as the AIC-best models with which to perform home-range estimation in 368 out of 369 datasets [34].

Ideally, a general theory to investigate the population-level consequences of range residency should recover a description of sessile organisms in the limit of vanishingly small home ranges and converge to nonspatial frameworks as home ranges increase in size and organisms explore them faster. Additionally, starting from an individual-level description of how organisms move and interact in space, this general theory should provide a dynamical equation for population abundance whose parameters contain information about home-range size and overlap. Encounter rates are the bridge between movement and population dynamics and thus provide a good starting point to upscale the consequences of movement to population dynamics. The first steps toward such a framework have focused, therefore, on deriving temporal and spatial statistics for the encounters between pairs of organisms with partially overlapping home ranges [9, 35]. Moreover, these first results already show that range-resident encounter rates can deviate significantly from law-of-mass-action expectations [9]. Yet, a complete upscaling embedding range-resident interactions into a birth/death population dynamics framework is still to be performed.

Here, we develop the range-resident logistic model as a unified spatial modeling framework linking individual movement behavior to its population-level consequences. In particular, the range-resident logistic model allows us to quantify how interactions between home range size, spatial distribution, and intraspecific competition affect population growth and carrying capacity. The proposed model uses OU stochastic process to represent movement and therefore captures the key features of range-resident movement and is supported by tracking data while still maintaining mathematical tractability. We also demonstrate how the range-resident logistic model includes both the classical logistic and spatial logistic models in the limits of very large and vanishingly small home range size, respectively. Importantly, we show that assuming well-mixed conditions may either under or overestimate population abundances. This new range-resident logistic framework thus unifies existing population dynamics models, providing important insights into how individual movement influences patterns observed at higher levels of organization.

2 Materials and Methods

2.1 The range-resident logistic model

We study a single-species population inhabiting a homogeneous habitat patch of area A and model its dynamics using an individual-based approach. The model incorporates different movement behaviors throughout the organism's lifetime and includes the minimum set of stochastic demographic processes required for density-dependent population growth: density-independent reproduction followed by dispersal and density-dependent death driven by intraspecific competition (Fig. 1). Apart from introducing range-resident movement, the model closely follows well-established logistic IBMs [31, 36].

Movement. We assume that changes in animal location occur on a much faster timescale (hours) than demographic processes (months to years), and animal trajectories are given by a continuous-in-time realization of a stochastic process (Fig. 1B). Under this assumption, movement is independent of any demographic process, and we can update the position of every organism in the population after each demographic event by integrating the stochastic differential equation that describes the movement process for each organism. Even though our focus is on how range residency influences population dynamics, we do not limit our analyses to range-resident movement. Instead, we consider the following movement behaviors:

- *Range-residency.* We use the Ornstein-Uhlenbeck (OU) process, a well-established stochastic model for range-resident animal movement supported by many tracking datasets [34]. OU movement accounts for the tendency of range-resident animals to return to the vicinity of a preferred location (home-range center), which leads to home ranges smaller than the population range and non-uniform patterns of space use within each home range. Assuming that movement is two-dimensional, isotropic, and uncorrelated in each of its components, the OU model is described mathematically by

$$\dot{\boldsymbol{x}}(t) = -\frac{1}{\tau}\big[\boldsymbol{x}(t) - \boldsymbol{\mu}\big] + \sqrt{\frac{2\sigma_r^2}{\tau}}\,\boldsymbol{\eta}(t) \tag{1}$$

  where $\boldsymbol{x}$ and $\boldsymbol{\mu}$ are two-dimensional vectors containing the organism and its home-range center locations, respectively; τ is the average home-range crossing time; and σ_r^2 defines the characteristic spatial scale of the home-range size by setting the long-term variance of the animal's space utilization function. $\boldsymbol{\eta}(t)$ is a two-dimensional white noise vector with zero-mean and unit-variance components. At sufficiently long time scales, the individual space utilization functions that result from the OU movement in Eq. (1) are isotropic Normal distributions with mean $\boldsymbol{\mu}$ and variance σ_r^2.

- *Uniform space usage.* To turn off the effect of range residency on the observed patterns of population dynamics, we also consider the simpler case in which organisms do not exhibit range residency and hence explore the whole population range. We can recover this movement behavior from Eq. (1) in the limit in which $\tau \to \infty$ and $\sigma_r^2 \to \infty$ with the diffusion coefficient $\sigma_r^2/\tau \equiv D$ finite [9].

- *Sessile.* Finally, we also consider the limit in which organisms do not move during their lifetime and thus remain where they land upon dispersal. In terms of parameter values, this limit corresponds to taking $\tau \to \infty$ and $\sigma_r^2 \to 0$ with the diffusion coefficient $D = 0$. In this limit, our model is equivalent to the spatial logistic model introduced by Bolker and Pacala, and Law *et al.* [31, 36].

Demographic processes.

- *Density-independent reproduction and dispersal.* Organisms in our model have a constant intrinsic birth rate b (Fig. 1A) and they disperse and establish their own home-range centers immediately upon birth. We sample the dispersal displacement between the offspring's home-range center and their parent's, $\boldsymbol{u}$, from a dispersal kernel, $\mathcal{K}^d(\boldsymbol{u})$. We use for this kernel a bivariate normal distribution centered on the parent's home-range center with standard deviation σ_d—the characteristic dispersal distance (Fig. 1A). For range-resident organisms, we additionally sample the initial position of the offspring from its asymptotic space utilization distribution, assuming that organisms relax to their steady-state movement behavior immediately after dispersal.

- *Density-dependent death.* We consider that organisms die at a rate that depends on how crowded their local environment is. For a focal organism i, its death rate is a function of its position $\boldsymbol{x}_i$, and is given by

$$d_i(\boldsymbol{x}_i) = d_0 + \gamma \sum_{j=1; j\neq i}^{N} \mathcal{K}^c(\boldsymbol{u}_{ij}) \tag{2}$$

where γ is the competition strength, N is the total number of organisms in the population, d_0 is the baseline death rate, and $\mathcal{K}^c(\boldsymbol{u}_{ij})$ is a competition kernel defining how competition intensity decays with the displacement between the focal organism i and its competing neighbor j (Fig. 1C). For the competition kernel, we choose a bivariate normal distribution (and thus normalized to one) with standard deviation σ_q, centered at the position of the focal organism i [36].

2.2 Analytical tools and approximations

2.2.1 Crowding Index

We use the crowding index $c(t)$ to quantify the effect of the spatial distribution of organisms on the population demographic rates. The crowding index is a weighted second-order spatial statistic using the competition kernel $\mathcal{K}^c$ as a weighting function

$$c(t) = \int_{\Omega} \mathcal{K}^c(\boldsymbol{u}) g_2(\boldsymbol{u}, t) \mathrm{d}\boldsymbol{u}, \tag{3}$$

where Ω labels the set of all possible displacements between organisms and $g_2(\boldsymbol{u}, t)$ is the population pair correlation function. This correlation function is a dimensionless second-order spatial metric measuring the ratio between the density of organism pairs separated by a displacement $\boldsymbol{u}$ and the average density of pairs, n^2 [37–39]—where n is the density of organisms $n = N/A$. Hence, $g_2(\boldsymbol{u}, t)$ is always equal or greater than zero, $g_2(\boldsymbol{u}, t) \geq 0$, for all $\boldsymbol{u}$. Specifically, when the spatial distribution of organisms is *complete spatial randomness* (CSR), organisms are homogeneously distributed in space and the density of pairs separated by any displacement $\boldsymbol{u}$ is equal to the average density of pairs. In this limit, the pair correlation function is constant and equal to one, $g_2^{\mathrm{CSR}}(\boldsymbol{u}, t) = 1$. Because the competition kernel is normalized, i.e. $\int_{\Omega} \mathcal{K}^c(\boldsymbol{u}) \mathrm{d}\boldsymbol{u} = 1$, the crowding index in this homogeneous-population limit is also equal to one. Index values greater than one indicate some degree of crowding within the population, and $c(t) < 1$ indicates over-dispersed populations at the competition scale.

This definition of the crowding index is similar to alternative definitions using the weighted covariance [31, 40]. The only difference is that we use the pair correlation function $g_2(\boldsymbol{u}, t)$ as the second-order spatial statistic instead of using the spatial covariance $\langle n(\boldsymbol{x}) - n, n(\boldsymbol{y}) - n \rangle$, where $n(\boldsymbol{x})$ is the local density of organisms at the position $\boldsymbol{x}$. Using the pair correlation function instead of the spatial covariance avoids the introduction of self-competition terms in the resulting population dynamics. The crowding index in terms of the weighted covariance, c_{cov}, is related to the crowding index defined in Eq. (3) by $c_{\mathrm{cov}} = n^2(c - 1)$.

2.2.2 Spatial moment dynamics equations

Spatial moment dynamics (SMD) is a mathematical method to approximate the dynamics of spatially explicit IBMs by a hierarchy of coupled ordinary differential equations describing the dynamics of the moments of the spatial distribution of organisms [33, 41–44]. This hierarchy of equations is often truncated at the second order, describing the coupled dynamics of the mean density of organisms (first moment) and the mean density of organism pairs separated by a displacement vector $\boldsymbol{u}$

(spatial correlations; second moment).

However, second-order SMD equations are hard to treat when each organism have its own home-range center. Alternatively, we worked with first-order SMD equations and treated spatial correlations via the crowding index, which also retains information on the local population density each organism experiences. To obtain the first-order SMD equation, we need first to derive the continuous equivalent of the discrete rates introduced in the IBM dynamics. Under our assumption of no net immigration or emigration, movement does not directly contribute to population size, and hence, the dynamics of the first spatial moment only depends on the balance between the birth and the death rate. The per-capita birth rate is constant and equal to b, whereas the per-capita death rate increases with local crowding accounting for intraspecific competition. To obtain these crowding effects, we need to compute the probability that a focal organism has a neighbor at a displacement $\boldsymbol{u}$, which is given by $ng_2(\boldsymbol{u})$ (see e.g., [33] for detailed derivations). Using this result, the per-capita death rate is

$$d(n) = d_0 + \gamma n \int_{\Omega} \mathcal{K}^c(\boldsymbol{u}) g_2(\boldsymbol{u}, t), \mathrm{d}\boldsymbol{u} \tag{4}$$

which allows us to obtain the dynamical equation for the density of organisms as

$$\frac{d}{dt} n(t) = [b - d(n)]\, n. \tag{5}$$

2.3 Numerical simulations

We simulated the IBM of Section 2.1 using Gillespie's algorithm [45], which we implemented in Python3 using the Numpy, Scipy, and Numba libraries [46–48]. The source code to reproduce all the data generated in the main text and supplementary figures is available at `https://github.com/r-menezes/logisticOU.git` and `https://doi.org/10.5281/zenodo.XXXX`. For each parameter combination, we ran 20 independent realizations, running each of them until the population reached a quasistationary state after 10^4 simulation events. We performed all simulations in a square domain of lateral length $L = 1$, using periodic boundary conditions and setting the reproduction, basal mortality, and interaction rates at $b = 1.1$, $d = 0.1$, and $\gamma = 0.002$, respectively. Other parameters were varied depending on the analyses, and their values are indicated in figure captions and legends. We initialized each simulation replicate with 500 organisms uniformly distributed in the spatial domain, which corresponds to the carrying capacity of the non-spatial model, $n^*_{\mathrm{CSR}} = (b - d)/\gamma$. To reduce the influence of the initial condition on the data collection, we discarded the data from each replicate's initial 4000 events. We tested that extending the simulation duration to $t_f = 500$ ($\approx 10^6$ simulation events) and recording data only for $400 < t \leq 500$ did not change the results.

Using this simulation setup, we obtained the population carrying capacity ($n_{t\to\infty}$), by averaging the population sizes measured at intervals of 400 events and finally taking the mean over realizations. We normalized $n_{t\to\infty}$, dividing it by n^*_{CSR} to highlight how the carrying capacity of the range-resident logistic model deviates from the homogeneous case.

3 Results

3.1 Numerical simulations of the range-resident logistic IBM

We first performed numerical simulations of the range-resident logistic IBM to understand how movement and spatial processes determine carrying capacity. Home-range size modulates the population carrying capacity, with larger home ranges leading to carrying capacities closer to that predicted by the non-spatial model (Fig. 2). For very large home ranges, organism movement is effectively Brownian (BM), with home ranges covering almost the entire simulation domain. In this limit, the population is homogeneously distributed in space, consistently with the non-spatial (or well-mixed) limit assumptions. For vanishingly small home ranges, organisms are effectively sessile (SS) and located at their home-range centers, with interaction rates depending only on the distance between home-range centers. Organisms whose home-range centers are close to each other interact much more strongly than pairs of organisms whose home-range centers are far away. Therefore, in this limit, the carrying capacity is strongly determined by the characteristic dispersal distance, σ_d: short-range dispersal led to population collapse, while the total abundance for long-range dispersal more than doubled that of homogenous populations (Fig. 2). Interestingly, the carrying capacity exhibited a minimum when home range, competition, and dispersal spatial scales were similar to each other, highlighting a non-trivial relationship between carrying capacity and home range size (orange line in Fig. 2).

Given the complex dependence of the carrying capacity on the various model parameters, we performed extensive simulations varying home-range size and crossing time, and competition and dispersal ranges over several orders of magnitude (Fig. 3). The competition range defines the scale at which organisms interact with each other, and thus has a strong impact on the carrying capacity. Long-range competition results in carrying capacities similar to that of the non-spatial model (rightmost column in Fig. 3). Short-range competition, however, leads to highly variable values of the carrying capacity (darker colors in the leftmost column of Fig. 3). Increasing the dispersal range generally leads to higher carrying capacities because offspring are more likely to establish new home ranges farther from their parents, which both avoids direct competition with them and increases the proportion of the available habitat the population colonizes (rows from bottom to top in Fig. 3). Finally, the carrying capacity is insensitive to changes in the home-range average crossing time,

except at very large values of τ for which the carrying capacity increases quickly with τ (y axes in Fig. 3). In this limit, organisms move very slowly and only explore a small fraction of their HRs before dying (see supplementary figure C.1). In contrast, when the home-range average crossing time is very short compared to the temporal scale of demographic dynamics, individual positions relax to their stationary probability distribution function between demographic events.

3.2 Mathematical expressions relating crowding, home-range overlap, and population size

To understand the relationship between the population carrying capacity and individual movement behavior, we constructed a first-order SMD approximation of the IBM and analyzed its equilibrium population sizes. As we showed in the Methods, the dynamics of the total density of organisms is given by

$$\frac{d}{dt}n(t) = \overbrace{b\,n(t)}^{\text{Birth}} \quad - \quad \overbrace{d\,n(t)}^{\text{Intrinsic death}} \quad - \quad \overbrace{\gamma c(t) n^2(t)}^{\text{Intraspecific competition}} \quad , \tag{6}$$

where $c(t)$ is the crowding index at time t defined in Eq. (3). If the population is homogeneously distributed in space, $c(t) = 1$ and the non-spatial logistic model is recovered [21]. Imposing $\frac{d}{dt}n = 0$ in Eq. (6) and solving for n returns two possible equilibria. The first one, $n_0^* = 0$, indicates population extinction. The second one is a non-trivial solution that defines the carrying capacity

$$n^* = \frac{(b-d)}{\gamma}\frac{1}{c^*} = \frac{n^*_{CSR}}{c^*}\,, \tag{7}$$

where c^* is the expected crowding index once the population reaches equilibrium. Equation (7) indicates that the ratio between the carrying capacities of the range-resident logistic model and the non-spatial model (n^*/n^*_{CSR}, depicted in Figs. 2-3) is equal to the inverse of the crowding index at equilibrium. The competition, dispersal, and movement spatial scales will thus affect the carrying capacity by modulating the population spatial distribution and hence changing crowding intensity. Each of these scales, however, plays a different role in defining crowding intensity. The competition kernel $\mathcal{K}^c$ is a weighting factor accounting for how strongly a given spatial configuration of organisms impacts the survival of a focal organism. Dispersal and movement behavior define the population spatial structure and, consequently, change the crowding index by altering the pair correlation function of organisms' positions $g_2(\boldsymbol{u}, t)$.

To explicitly investigate how crowding depends on movement behavior, we redefine the crowding index in terms of the size and distribution of home ranges in space. Thus, we calculate the crowding index based on the PCF of the point pattern of organisms' home range centers $g_2^{\mathrm{HR}}(\boldsymbol{u}, t)$. In this

case, the weighting function will depend both on the competition kernel and on the pattern of space usage of each organism around its home range center, which we assume to be constant across the population in our simulations. Denoting the weighting function for the crowding of home ranges as $\mathcal{K}^{\mathrm{HR}}(\boldsymbol{u})$, it follows that

$$c_{\mathrm{HR}}(t) = \int \mathcal{K}^{\mathrm{HR}}(\boldsymbol{u}) g_2^{\mathrm{HR}}(\boldsymbol{u}, t) \mathrm{d}\boldsymbol{u} \ . \tag{8}$$

For the common case in which range-resident animals have mean home-range crossing times much shorter than the demographic time scales, i.e. $\tau \ll b + d$, Eq. (8) is equivalent to (3) (see supplementary material A) and our range-resident logistic model is equivalent to a version of the (sessile) spatial logistic model with modified competition kernels [31, 36]. Specifically, if interactions among organisms are local, i.e. $\mathcal{K}^c(\boldsymbol{u}) \to \delta(\boldsymbol{u})$, the range-resident logistic model is equivalent to a model of "sessile organisms" (the home range centers) interacting via a competition kernel that is defined by the stationary distribution of displacements between organisms (i.e., the distribution of displacements between organisms when organism locations are sampled from the space utilization distribution, see supplementary material A). This relationship thus provides a mathematical expression relating crowding, and consequently the total population size, to home-range overlap.

3.3 Crowding indexes as predictors of total population size

Finally, we tested the accuracy of the crowding index in predicting the carrying capacity of the population. From equation (7), the inverse of the crowding index is equal to the normalized carrying capacity, and thus provides a way to anticipate the population carrying capacity using only spatial information. We measured the crowding index using the competition scale and either information about organism locations or HRs' centers and size for a large subset of simulations (Fig. 3 panels d-i; see supplementary material B). We compared the normalized carrying capacity measured in the simulations with the inverse of the measured crowding index in a predicted versus measured diagram (Fig. 4). We initially did not consider small interaction scales in these results, ($\sigma_q = 10^{-3}$, Fig. 3 panels a-c) because local interactions are associated with very large effective interaction rates when organisms are close together and thus introduce deviations from our theory that considers mean interaction rates [49, 50]. The predicted and measured carrying capacities showed a remarkable similarity ($R^2 = 0.969$ for c^*_{pos} and $R^2 = 0.946$ for c^*_{HR}). Including small interaction scales in the analysis decreased the accuracy of predictions, but the crowding index still explained most of the variance in the data ($R^2 = 0.823$ for c^*_{pos} and $R^2 = 0.812$ for c^*_{HR}, supplementary figure C.2). These results indicate that the crowding index, even when computed entirely using movement parameters that describe long-term animal movement, is a reliable predictor of the carrying capacity of the

population.

4 Discussion

We generalized existing spatial logistic models [31, 36] to include the two main features of range-resident movement: organisms moving within home ranges that are smaller than the population range and exhibiting uneven patterns of space use. These two features introduce a tradeoff between how strongly and how far organisms interact with one another. Larger home ranges increase the number of potential interactions for a focal organism but make each potential interaction with a particular competitor less frequent and weaker on average. This tradeoff can lead to non-monotonic relationships between home-range size and carrying capacity, and is particularly relevant when home-range sizes are comparable to the spatial scales of dispersal and competition. When home ranges are very large, organisms are homogeneously distributed and interactions are well described by the law of mass action. Conversely, when home ranges are very small, organisms are effectively sessile and the population size is entirely determined by the competition and dispersal scales. Hence, this new framework captures two of the existing formulations of the logistic model as limits. It recovers the spatial logistic equations for sessile organisms when home ranges are vanishingly small [31, 36] and Verhulst's original formulation when home ranges are infinitely large [21].

The simplicity of this new formalism allowed us to derive mathematical relationships that link home-range size and home-range overlap to determine intraspecific interactions and, ultimately, population size. Specifically, in the most realistic regime in which home-range crossing times are much shorter than the typical times between demographic events—so animal movement is stationary within the organism's lifetime [51]—and the width of the competition kernel is negligible compared to the home-range size [9], intraspecific interactions are entirely determined by the long-term spatial pattern of individual space use. This is one of our key results, and it connects the strength of intraspecific interactions to movement parameters for which robust statistical estimators exist [5].

Importantly, home-range overlap determines competition intensity via the convolution of organisms' space utilization functions, and thus incorporates information about typical distances between organisms. This information is missing in metrics of home-range overlap that are commonly used to quantify the strength of interactions between individuals, such as the Bhattacharyya coefficient [9], and could lead to overlap metrics either over and underestimating interaction strengths depending on individual home-range sizes and spatial configurations. Leveraging this information about how individual patterns of space use determine the strength of intraspecific interactions, we generalized the crowding index, first introduced to study interactions in plant communities [31, 52], to motile organisms and showed that it accurately predicts the effect of population spatial structure on pop-

ulation's carrying capacity. This generalization defines the regimes where range-resident animals can be described as sessile organisms with an associated interaction kernel given by their space utilization distribution. Therefore, it connects the mathematical framework underlying neighborhood models in plant ecology with animal population and community dynamics in range-resident species [53, 54].

The crowding index has already been successfully used to integrate spatial information into demographic models for species-rich plant communities [38, 52]. Our generalization of this index could be used similarly for motile organisms, harnessing the availability of animal tracking data to inform interactions and build a bridge between movement ecology and population dynamics. Conversely, the crowding index could provide a simple path to extend existing models of population and community dynamics to incorporate the movement behavior and spatial distribution of organisms. This approach could be useful for reconstructing spatial interaction networks from co-occurrence data without assuming that interaction coefficients are proportional to population range overlap [55, 56], which could yield misleading results, as we discussed above.

The range-resident logistic model we propose results from a compromise between incorporating real-world complexity and maintaining a level of abstraction that allows for general insights. Besides its most obvious extension to a larger number of competing species and interactions, our framework can be refined to incorporate additional features of individual movement and life history traits. We list a few here, remarking that most of them would likely make the model mathematically intractable. Firstly, considering home range variability over time for a single individual and across individuals within the population [57, 58], together with variability of life history parameters such as reproduction and death rates, our new approach could be used to investigate how individual variability shapes spatiotemporal population dynamics [28, 29]. Secondly, by including environmental heterogeneity, perception, and navigation [sensu 59], one could explore connections between resource spatial distributions, carrying capacity, and population spatial structure. Additional extensions linking birth rates to home range size and resource availability could also prove fruitful in relating environmental quality to carrying capacities [60]. Thirdly, neighborhood-biased or cross-correlated movement could increase the realism of the model for many populations. This could provide a way to link mechanistic home range analyses to the framework we propose [61, 62], as well as to investigate how avoidance/attraction to conspecifics could change the carrying capacity of a population [63]. Lastly, further developments overcoming the simplified dispersal dynamics based on a dispersal kernel [64, 65] could be used to investigate the interplay between home range establishment and fidelity. In particular, incorporating different aspects of habitat selection during the establishment phase [66] and over the course of organisms' lives would be a way of exploring connections with multiple aspects of behavior.

In summary, we showed that accounting for range residency, a widespread feature of animal movement, is key to better understanding spatial patterns of aggregation, intensity of intraspecific interactions, and, ultimately, population dynamics. We established the theoretical foundation to formalize these relationships, and provided mathematical expressions relating movement parameters, accessible from animal tracking data, to local crowding metrics and long-term population sizes in a single-species model of population dynamics. This new framework, moreover, recovers previous formulations of the logistic model simply by manipulating home-range sizes, thus providing a unifying theory to study population dynamics in sessile, range-resident, and free-ranging species. Finally, because our theory balances ecological realism with mathematical tractability, it constitutes an important step toward the long-standing goal of bridging movement and population ecology.

Acknowledgements

This study was financed in part by the National Council for Scientific and Technological Development, Brazil - CNPq: 140096/2021-3 (R.M.) and by the Coordenação de Aperfeiçoamento de Pessoal de Nível Superior - Brasil (CAPES) - Finance Code 001 (R.M.); This work was partially funded by the Center for Advanced Systems Understanding (CASUS), which is financed by Germany's Federal Ministry of Education and Research (BMBF) and by the Saxon Ministry for Science, Culture and Tourism (SMWK) with tax funds on the basis of the budget approved by the Saxon State Parliament; the São Paulo Research Foundation (FAPESP, Brazil) through BIOTA Young Investigator Research Grant No. 2019/05523-8 (R.M-G); ICTP-SAIFR grant no. 2021/14335-0 (R.M. and R.M.-G); the Simons Foundation through grant no. 284558FY19 (R.M-G). The National Science Foundation (NSF, USA) grant DBI_al_1915347 supported the involvement of J.M.C. and W.F.F. This research was supported by resources supplied by the Center for Scientific Computing (NCC/GridUNESP) of the São Paulo State University (UNESP).

Authorship

R.M and R.M.-G conceived the project and developed the model. R.M. performed all numerical and mathematical analyses with input from R.M.-G and P.I.P. R.M. and R.M.-G wrote the manuscript with input from all other authors. All authors discussed ideas and the results, and gave final approval for paper publication.

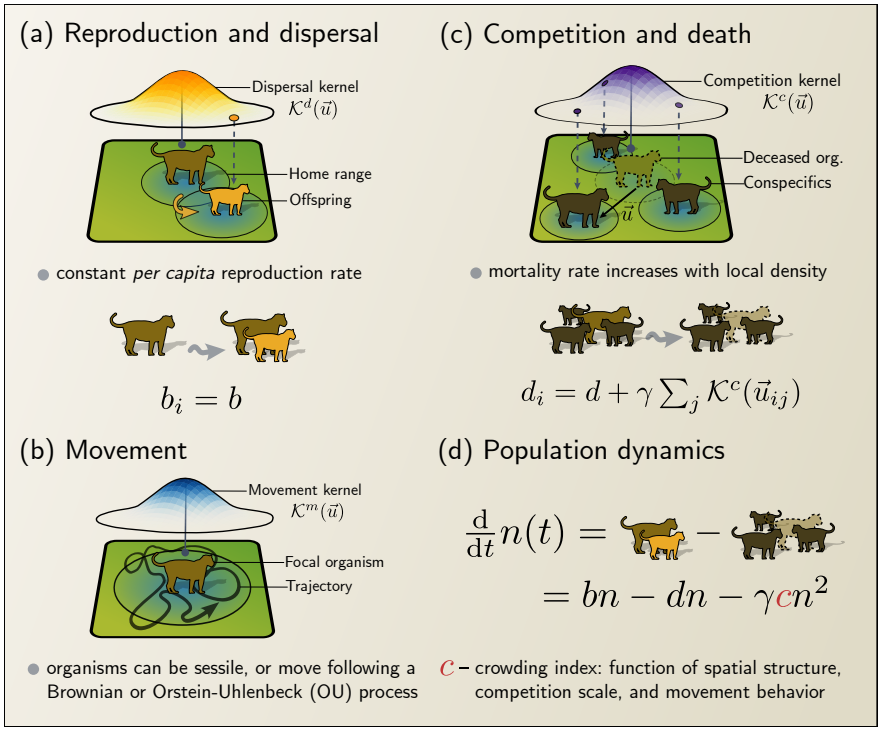

Figure 1: Graphical summary of the range-resident logistic model. (a) Organisms reproduce at a constant rate b with offspring establishing new home ranges (HR) at a position sampled from a juvenile dispersal kernel, $\mathcal{K}^d(\boldsymbol{u})$, centered at the parent's home range center. (b) Organisms move following stochastic movement models. After each simulation step, the position of the organisms were updated by integrating the corresponding stochastic differential equation. (c) Organisms experience a baseline mortality rate of d that grows linearly with the local density of organisms. This local density around each organism is calculated using a competition kernel $\mathcal{K}^c(\boldsymbol{u})$. (d) Population abundance changes over time due to the balance between birth and death. Spatial factors such as movement and dispersal change the aggregation pattern, measured by the crowding index c.

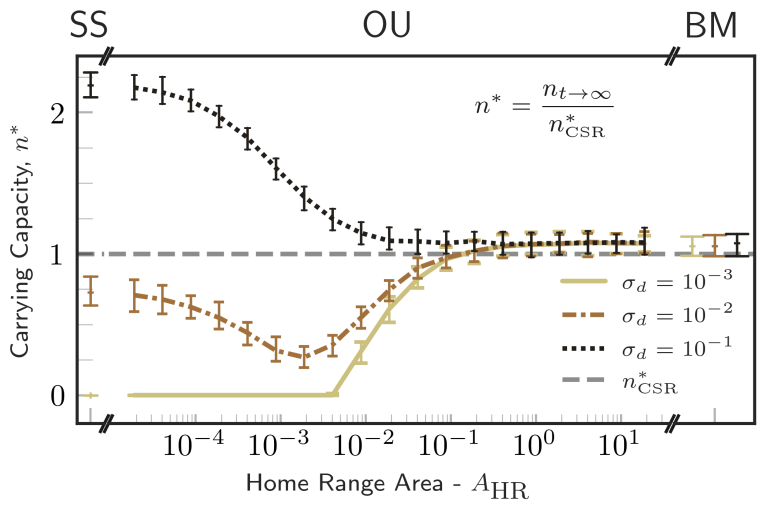

Figure 2: Home-range size is a key driver of the population carrying capacity. The carrying capacity, measured directly from IBM simulations and scaled by the homogeneous carrying capacity $n^*_{\mathrm{CSR}} = (b-d)/\gamma$ (gray-dashed line), versus home-range size. Different colors represent different dispersal ranges, as indicated in the legend. Curves and vertical bars correspond to the median and 90% percentile interval of the carrying capacity measured across realizations with the same parameter set. The labels on the top indicate the movement model used in the simulations: sessile (SS), range-resident movement (Orstein-Uhlenbeck; OU), and uniform space use (Brownian movement; BM). For OU movement, we changed the home-range area by increasing home-range crossing times while keeping diffusion fixed. When the home-range area and dispersal were small, populations go extinct.

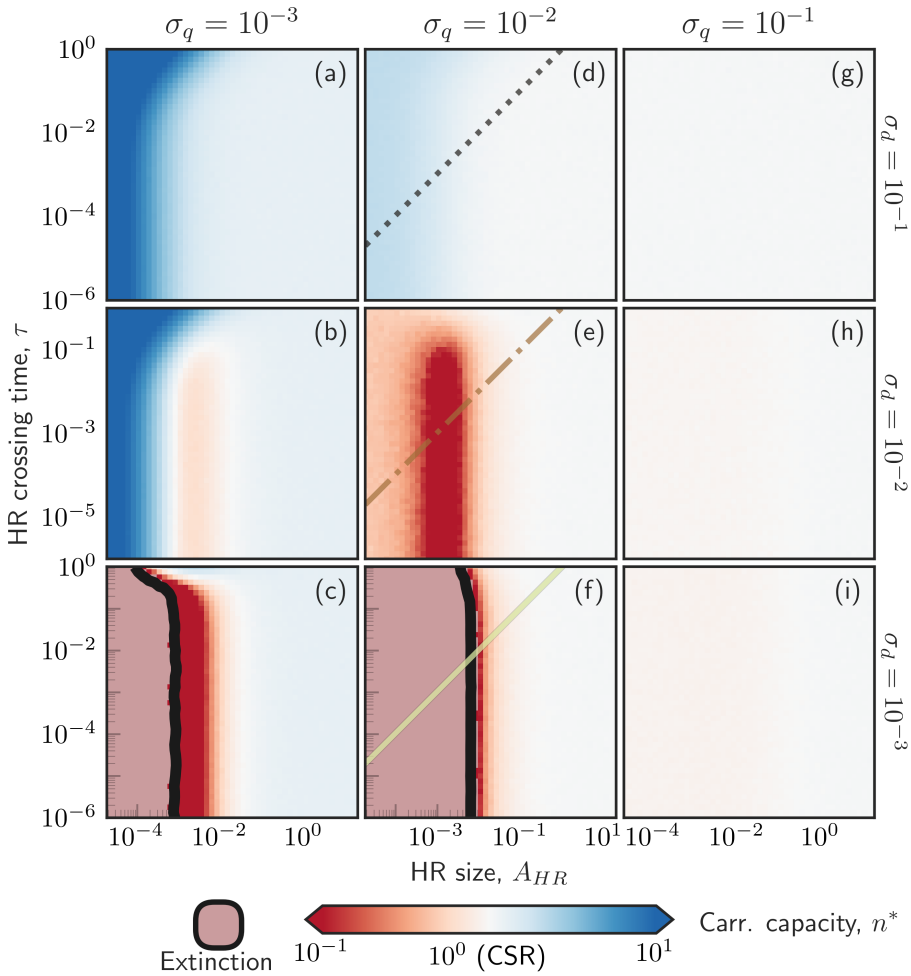

Figure 3: Competition and dispersal scales change the carrying capacity of the population across varying home-range sizes and crossing times. Across all panels, the carrying capacity of the population measured from simulations ($n^* = n_{t\to\infty}/n^*_{\mathrm{CSR}}$) is plotted against the HR size (bottom axes), the HR crossing time (left axes), the competition scale (columns; top axis), and the juvenile dispersal scale (rows; right axis). Increasing HR size or competition range leads effectively to non-spatial dynamics, regardless of the value of other model parameters (lighter colors in the heatmaps). The HR average crossing time τ does not change the carrying capacity, except for large τ and small HRs where organisms are effectively sessile. Increasing juvenile dispersal allows for larger population abundances across all the parameter ranges considered. The colored lines in the central column indicate the parameter combinations used in Fig. 2, following the same color code used there.

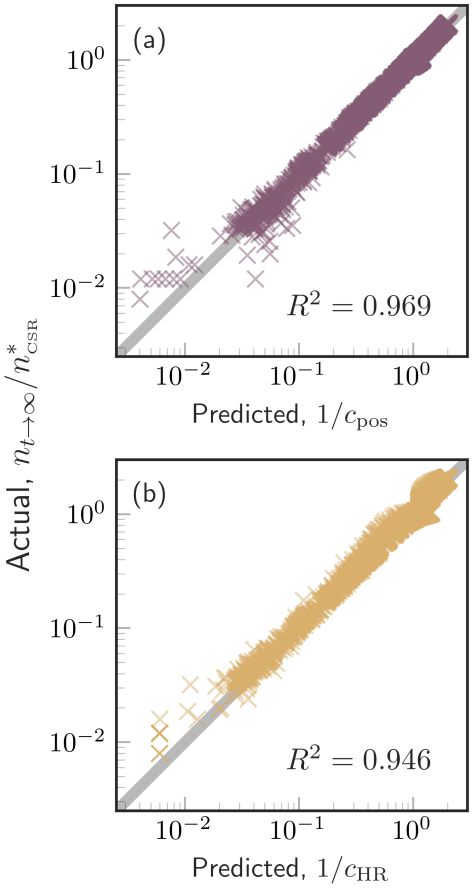

Figure 4: Crowding indexes accurately predict population carrying capacity. (a) The crowding index measured using organism locations in simulation snapshots. (b) The crowding index measured based on the expected mortality rate an organism experiences given its home range size and distances between home-range centers.Gray lines in the background of each panel represent the complete agreement (1-1 line), and R^2 values are provided as indicators of the goodness of the linear fit.

References

[1] Kranstauber B, Cameron A, Weinzerl R, Fountain T, Tilak S, Wikelski M, et al. The Movebank Data Model for Animal Tracking. Environmental Modelling & Software. 2011 Jun;26(6):834-5.

[2] Kays R, Crofoot MC, Jetz W, Wikelski M. Terrestrial animal tracking as an eye on life and planet. Science. 2015;348(6240):aaa2478.

[3] Langley LP, Lang SDJ, Ozsanlav-Harris L, Trevail AM. ExMove: An Open-Source Toolkit for Processing and Exploring Animal-Tracking Data in R. Journal of Animal Ecology. 2024;93(7):784-95.

[4] McClintock BT, Langrock R, Gimenez O, Cam E, Borchers DL, Glennie R, et al. Uncovering Ecological State Dynamics with Hidden Markov Models. Ecology Letters. 2020;23(12):1878-903.

[5] Silva I, Fleming CH, Noonan MJ, Alston J, Folta C, Fagan WF, et al. Autocorrelation-informed Home Range Estimation: A Review and Practical Guide. Methods in Ecology and Evolution. 2022 Mar;13(3):534-44.

[6] Burt WH. Territoriality and Home Range Concepts as Applied to Mammals. Journal of Mammalogy. 1943 Aug;24(3):346-52.

[7] Berger KM, Gese EM. Does interference competition with wolves limit the distribution and abundance of coyotes? Journal of animal Ecology. 2007;76(6):1075-85.

[8] Powell RA. Mustelid spacing patterns: variations on a theme by Mustela. Zeitschrift für Tierpsychologie. 1979;50(2):153-65.

[9] Martinez-Garcia R, Fleming CH, Seppelt R, Fagan WF, Calabrese JM. How Range Residency and Long-Range Perception Change Encounter Rates. Journal of Theoretical Biology. 2020 Aug;498:110267.

[10] Fagan WF, Krishnan A, Liao Q, Fleming CH, Liao D, Lamb C, et al. Intraspecific Encounters Can Lead to Reduced Range Overlap. Movement Ecology. 2024 Dec;12(1):1-13.

[11] Doncaster CP. Non-parametric estimates of interaction from radio-tracking data. Journal of Theoretical Biology. 1990 Apr;143(4):431-43. Available from: https://linkinghub.elsevier.com/retrieve/pii/S0022519305800207.

[12] Fieberg J, Kochanny CO. Quantifying home-range overlap: the importance of the utilization distribution. Journal of Wildlife Management. 2005 Oct;69(4):1346-59. Available from: http://www.bioone.org/doi/abs/10.2193/0022-541X%282005%2969%5B1346%3AQHOTIO%5D2.0.CO%3B2.

[13] Winner K, Noonan MJ, Fleming CH, Olson KA, Mueller T, Sheldon D, et al. Statistical Inference for Home Range Overlap. Methods in Ecology and Evolution. 2018;9(7):1679-91.

[14] Knapton RW, Krebs JR. Settlement Patterns, Territory Size, and Breeding Density in the Song Sparrow (Melospiza Melodia). Canadian Journal of Zoology. 1974 Nov;52(11):1413-20.

[15] López-Sepulcre A, Kokko H. Territorial Defense, Territory Size, and Population Regulation. The American Naturalist. 2005 Sep;166(3):317-25.

[16] Ayllón D, Almodóvar A, Nicola GG, Parra I, Elvira B. Modelling Carrying Capacity Dynamics for the Conservation and Management of Territorial Salmonids. Fisheries Research. 2012 Dec;134–136:95-103.

[17] Doherty PJ. Tropical Territorial Damselfishses: Is Density Limited by Aggression or Recruitment? Ecology. 1983;64(1):176-90.

[18] Hartmann SA, Oppel S, Segelbacher G, Juiña ME, Schaefer HM. Decline in Territory Size and Fecundity as a Response to Carrying Capacity in an Endangered Songbird. Oecologia. 2017 Feb;183(2):597-606.

[19] Morales JM, Moorcroft PR, Matthiopoulos J, Frair JL, Kie JG, Powell RA, et al. Building the Bridge between Animal Movement and Population Dynamics. Philosophical Transactions of the Royal Society B: Biological Sciences. 2010 Jul;365(1550):2289-301.

[20] Costa-Pereira R, Moll RJ, Jesmer BR, Jetz W. Animal Tracking Moves Community Ecology: Opportunities and Challenges. Journal of Animal Ecology. 2022 Apr;00:1-11.

[21] Verhulst PF. Notice Sur La Loi Que La Population Suit Dans Son Accroissement. Correspondence Mathématique et Physique. 1838;10:113-26.

[22] Lotka AJ. Contribution to the Mathematical Theory of Capture. Proceedings of the National Academy of Sciences of the United States of America. 1932 Feb;18(2):172-8.

[23] Hutchinson JMC, Waser PM. Use, Misuse and Extensions of "Ideal Gas" Models of Animal Encounter. Biological Reviews. 2007;82(3):335-59.

[24] Hanski I. Metapopulation Dynamics. Nature. 1998 Nov;396(6706):41-9.

[25] Cantrell RS, Cosner C. Spatial ecology via reaction-diffusion equations. John Wiley & Sons; 2004.

[26] Grimm V, Railsback SF. Individual-based modeling and ecology. Princeton University Press; 2013.

[27] Giuggioli L, Potts JR, Harris S. Animal Interactions and the Emergence of Territoriality. PLoS Computational Biology. 2011 Mar;7(3):e1002008.

[28] Milles A, Dammhahn M, Grimm V. Intraspecific Trait Variation in Personality-Related Movement Behavior Promotes Coexistence. Oikos. 2020;129(10):1441-54.

[29] Buchmann CM, Schurr FM, Nathan R, Jeltsch F. An Allometric Model of Home Range Formation Explains the Structuring of Animal Communities Exploiting Heterogeneous Resources. Oikos. 2011;120(1):106-18.

[30] Buchmann CM, Schurr FM, Nathan R, Jeltsch F. Movement Upscaled – the Importance of Individual Foraging Movement for Community Response to Habitat Loss. Ecography. 2012;35(5):436-45.

[31] Bolker B, Pacala SW. Using Moment Equations to Understand Stochastically Driven Spatial Pattern Formation in Ecological Systems. Theoretical Population Biology. 1997 Dec;52(3):179-97.

[32] Dieckmann U, Law R, Metz JAJ, editors. The Geometry of Ecological Interactions: Simplifying Spatial Complexity. 1st ed. Cambridge University Press; 2000.

[33] Plank MJ, Law R. Spatial Point Processes and Moment Dynamics in the Life Sciences: A Parsimonious Derivation and Some Extensions. Bulletin of Mathematical Biology. 2015 Apr;77(4):586-613.

[34] Noonan MJ, Tucker MA, Fleming CH, Akre TS, Alberts SC, Ali AH, et al. A Comprehensive Analysis of Autocorrelation and Bias in Home Range Estimation. Ecological Monographs. 2019;89(2):e01344.

[35] Noonan MJ, Martinez-Garcia R, Davis GH, Crofoot MC, Kays R, Hirsch BT, et al. Estimating Encounter Location Distributions from Animal Tracking Data. Methods in Ecology and Evolution. 2021;12(7):1158-73.

[36] Law R, Murrell DJ, Dieckmann U. Population Growth in Space and Time: Spatial Logistic Equations. Ecology. 2003;84(1):252-62.

[37] Law R, Illian J, Burslem DFRP, Gratzer G, Gunatilleke CVS, Gunatilleke IaUN. Ecological Information from Spatial Patterns of Plants: Insights from Point Process Theory. Journal of Ecology. 2009;97(4):616-28.

[38] Wiegand T, Wang X, Fischer S, Kraft NJB, Bourg NA, Brockelman WY, et al.. Latitudinal Scaling of Aggregation with Abundance and Its Consequences for Coexistence in Species Rich Forests. bioRxiv; 2023.

[39] Baddeley A, Rubak E, Turner R. Spatial Point Patterns: Methodology and Applications with R. Champan & Hall/CRC Interdisciplinary Statistics Series. Boca Raton ; London ; New York: CRC Press, Taylor & Francis Group; 2016.

[40] Bolker BM, Pacala SW. Spatial Moment Equations for Plant Competition: Understanding Spatial Strategies and the Advantages of Short Dispersal. The American Naturalist. 1999;153(6):575-602.

[41] Markham DC, Simpson MJ, Maini PK, Gaffney EA, Baker RE. Incorporating Spatial Correlations into Multispecies Mean-Field Models. Physical Review E. 2013 Nov;88(5):052713.

[42] Murrell DJ, Dieckmann U, Law R. On Moment Closures for Population Dynamics in Continuous Space. Journal of Theoretical Biology. 2004 Aug;229(3):421-32.

[43] Simpson MJ, Sharp JA, Baker RE. Distinguishing between Mean-Field, Moment Dynamics and Stochastic Descriptions of Birth–Death–Movement Processes. Physica A: Statistical Mechanics and its Applications. 2014 Feb;395:236-46.

[44] Iwasa Y. Lattice Models and Pair Approximation in Ecology. In: Metz JAJ, Law R, Dieckmann U, editors. The Geometry of Ecological Interactions: Simplifying Spatial Complexity. Cambridge Studies in Adaptive Dynamics. Cambridge: Cambridge University Press; 2000. p. 227-51.

[45] Gillespie DT. Exact Stochastic Simulation of Coupled Chemical Reactions. The Journal of Physical Chemistry. 1977 Dec;81(25):2340-61.

[46] Harris CR, Millman KJ, van der Walt SJ, Gommers R, Virtanen P, Cournapeau D, et al. Array Programming with NumPy. Nature. 2020 Sep;585(7825):357-62.

[47] Virtanen P, Gommers R, Oliphant TE, Haberland M, Reddy T, Cournapeau D, et al. SciPy 1.0: Fundamental Algorithms for Scientific Computing in Python. Nature Methods. 2020 Mar;17(3):261-72.

[48] Lam SK, Pitrou A, Seibert S. Numba: A LLVM-based Python JIT Compiler. In: Proceedings of the Second Workshop on the LLVM Compiler Infrastructure in HPC. LLVM '15. New York, NY, USA: Association for Computing Machinery; 2015. p. 1-6.

[49] de Figueiredo BG, Calabrese JM, Fagan WF, Martinez-Garcia R. The Structure of Inter-Reaction Times in Reaction-Diffusion Processes and Consequences for Counting Statistics. arXiv; 2024.

[50] Das D, Kenkre VM, Nathan R, Giuggioli L. Misconceptions about Quantifying Animal Encounter and Interaction Processes. Frontiers in Ecology and Evolution. 2023 Oct;11:1230890.

[51] Fleming CH, Calabrese JM, Mueller T, Olson KA, Leimgruber P, Fagan WF. From Fine-Scale Foraging to Home Ranges: A Semivariance Approach to Identifying Movement Modes across Spatiotemporal Scales. The American Naturalist. 2014 May;183(5):E154-67. Publisher: University of Chicago PressChicago, IL ISBN: 00030147. Available from: https://www.journals.uchicago.edu/doi/10.1086/675504.

[52] Wiegand T, Wang X, Anderson-Teixeira KJ, Bourg NA, Cao M, Ci X, et al. Consequences of Spatial Patterns for Coexistence in Species-Rich Plant Communities. Nature Ecology & Evolution. 2021 Jul;5(7):965-73.

[53] Silander JA, Pacala SW. Neighborhood Predictors of Plant Performance. Oecologia. 1985 May;66(2):256-63.

[54] Pacala SW, Silander JA. Neighborhood Models of Plant Population Dynamics. I. Single-Species Models of Annuals. The American Naturalist. 1985 Mar;125(3):385-411.

[55] Galiana N, Arnoldi JF, Mestre F, Rozenfeld A, Araújo MB. Power Laws in Species' Biotic Interaction Networks Can Be Inferred from Co-Occurrence Data. Nature Ecology & Evolution. 2024;8(2):209-17.

[56] Thompson L, Galiana N, Wells K, Lurgi M. Protected Areas Enhance Avian Food Webs. bioRxiv; 2023.

[57] Ellison N, Hatchwell BJ, Biddiscombe SJ, Napper CJ, Potts JR. Mechanistic Home Range Analysis Reveals Drivers of Space Use Patterns for a Non-Territorial Passerine. Journal of Animal Ecology. 2020;89(12):2763-76.

[58] Fleming CH, Deznabi I, Alavi S, Crofoot MC, Hirsch BT, Medici EP, et al. Population-level Inference for Home-range Areas. Methods in Ecology and Evolution. 2022 May;13(5):1027-41.

[59] Nathan R, Getz WM, Revilla E, Holyoak M, Kadmon R, Saltz D, et al. A Movement Ecology Paradigm for Unifying Organismal Movement Research. Proceedings of the National Academy of Sciences. 2008 Dec;105(49):19052-9.

[60] Carter N, Levin S, Barlow A, Grimm V. Modeling Tiger Population and Territory Dynamics Using an Agent-Based Approach. Ecological Modelling. 2015 Sep;312:347-62.

[61] Potts JR, Lewis MA. How Do Animal Territories Form and Change? Lessons from 20 Years of Mechanistic Modelling. Proceedings of the Royal Society B: Biological Sciences. 2014 Jun;281(1784):20140231.

[62] Moorcroft PR, Lewis MA. Mechanistic Home Range Analysis. (MPB-43). Princeton University Press; 2013.

[63] Surendran A, Plank MJ, Simpson MJ. Spatial Structure Arising from Chase-Escape Interactions with Crowding. Scientific Reports. 2019 Oct;9(1):14988.

[64] Bullock JM, Mallada González L, Tamme R, Götzenberger L, White SM, Pärtel M, et al. A Synthesis of Empirical Plant Dispersal Kernels. Journal of Ecology. 2017;105(1):6-19.

[65] Rogers HS, Beckman NG, Hartig F, Johnson JS, Pufal G, Shea K, et al. The Total Dispersal Kernel: A Review and Future Directions. AoB PLANTS. 2019 Sep;11(5):plz042.

[66] Mayor SJ, Schneider DC, Schaefer JA, Mahoney SP. Habitat Selection at Multiple Scales. Écoscience. 2009 Jun;16(2):238-47.

[67] Wiegand T, Moloney KA. Handbook of Spatial Point-Pattern Analysis in Ecology. Boca Raton: CRC Press, Taylor & Francis Group; 2014.

Supporting Information

A The crowding index for home range centers.

In this appendix, we derive the expression for the crowding index based on home-range centers, Eq. (8), starting from its definition in terms of the instantaneous organism location, Eq. (3).

The position of a focal organism, i, and the displacement between this organism i and a neighbor j, both at time t, can be represented by two random variables $X_t^{(i)}$ and $U_t^{(i,j)} = X_t^{(j)} - X_t^{(i)}$, respectively. Each of these random variables has a probability density function (PDF), $f_{X_t^{(i)}}(\boldsymbol{x})$ and $f_{U_t^{(i,j)}}(\boldsymbol{u})$, respectively. Similarly, we denote each individual's home-range center as $\bar{X}^{(i)}$, the displacement of the organism from its home range center at time t as $Y_t^{(i)}$, and the displacement between a pair of organisms' home-range centers as $\bar{U}^{(i,j)}$. Using these definitions, the displacement between organisms is

$$U_t^{(i,j)} = X_t^{(j)} - X_t^{(i)} = X_t^{(j)} - X_t^{(i)} \pm \overline{X}^{(i)} \pm \overline{X}^{(j)} = Y_t^{(j)} - Y_t^{(i)} + \overline{U}^{(i,j)} \,. \tag{A.1}$$

Because the PDF of a sum of random variables is the convolution of the PDFs of the random variables, the PDF of the displacement between organisms at time t is given by the convolution of PDF associated to $Y_t^{(j)}$, $-Y_t^{(i)}$ and $\overline{U}^{(i,j)}$. Mathematically, and using f to denote all PDFs, we can write this relationship as

$$f_{U_t^{(i,j)}}(\boldsymbol{u}, t) = \left(f_{-Y_t^{(i)}} * f_{Y_t^{(j)}} * f_{\overline{U}^{(i,j)}} \right)(\boldsymbol{u}, t). \tag{A.2}$$

Additionally, the distribution of displacements between organisms i and j, averaged over all possible pairs of organisms, is directly related to the pair correlation function $g_2(\boldsymbol{u}, t)$

$$g_2(\boldsymbol{u}, t) = \frac{A}{N(N-1)} \sum_{i \neq j} f_{U^{(i,j)}}(\boldsymbol{u}, t) \tag{A.3}$$

$$= \frac{A}{N(N-1)} \sum_{i \neq j} \left(f_{-Y_t^{(i)}} * f_{Y_t^{(j)}} * f_{\overline{U}^{(i,j)}} \right)(\boldsymbol{u}, t) \,. \tag{A.4}$$

For range-resident organisms, the distribution of their position around its center tends to a constant asymptotic distribution directly related to its movement behavior, i.e. $f_{Y^{(i)}_{t\to\infty}} = f_{Y^{(i)}}$ for any organism i. If we further assume that the home ranges of organisms are identical ($f_{Y^{(i)}} = f_{Y^{(j)}} = f_Y \, \forall \, i, j$) and symmetric ($f_{-Y} = f_Y$), we can use the linearity of the convolution to write

$$g_2(\boldsymbol{u},t) = \left(f_Y * f_Y * \frac{A}{N(N-1)} \sum_{i \neq j} f_{\overline{U}^{(i,j)}} \right)(\boldsymbol{u},t) \tag{A.5}$$

$$g_2(\boldsymbol{u},t) = \left(f_Y * f_Y * g_2^{\mathrm{HR}}(\boldsymbol{u},t) \right)(\boldsymbol{u},t)\,, \tag{A.6}$$

where we can identify $g_2^{\mathrm{HR}}(\boldsymbol{u},t) = \frac{A}{N(N-1)} \sum_{i \neq j} f_{\overline{U}^{(i,j)}}$ with the home-range center pair correlation function.

Finally, using Eq. (A.6), we can rewrite the crowding index as

$$c(t) = \int_\Omega \mathcal{K}(\boldsymbol{u}) g_2(\boldsymbol{u},t) \mathrm{d}\boldsymbol{u} \tag{A.7}$$

$$= \int_\Omega \mathcal{K}(\boldsymbol{u}) \left(f_Y * f_Y * g_2^{\mathrm{HR}}(\boldsymbol{u},t) \right)(\boldsymbol{u},t) \mathrm{d}\boldsymbol{u} \tag{A.8}$$

$$= \int_\Omega \left(\mathcal{K} * f_Y * f_Y \right)(\boldsymbol{u}) g_2^{\mathrm{HR}}(\boldsymbol{u},t) \mathrm{d}\boldsymbol{u} \tag{A.9}$$

$$c_{\mathrm{HR}}(t) = \int_\Omega \mathcal{K}^{\mathrm{HR}}(\boldsymbol{u}) g_2^{\mathrm{HR}}(\boldsymbol{u},t) \mathrm{d}\boldsymbol{u}\,, \tag{A.10}$$

where we define the home range competition kernel $\mathcal{K}^{\mathrm{HR}}(\boldsymbol{u}) = \left(\mathcal{K} * f_Y * f_Y \right)(\boldsymbol{u})$ and we denote the crowding index with the subscript HR to highlight that it is calculated using the distribution of HR centers instead of the using the spatial distribution of organisms.

B Measurement of the crowding index using spatial information.

This appendix explains how to measure the crowding index from simulation data. A simulation snapshot showing the spatial distribution of organisms can be described as a N-point pattern $P = \{\boldsymbol{x}_i\}$ in which $\boldsymbol{x}_i$ denotes the coordinates of the i-th point. Ignoring edge corrections because we are working with toroidal spatial domains, the pair correlation function of such point pattern is [39, 67]:

$$\hat{g}_2(\boldsymbol{u}) = \frac{1}{N(N-1)} \sum_{i \neq j} \delta\left(\boldsymbol{u} - \boldsymbol{x}_j + \boldsymbol{x}_i \right)\,, \tag{B.1}$$

where $\delta(\boldsymbol{u})$ is the Dirac delta distribution and the summation is over all possible pairs of organisms. Substituting equation (B.1) into Eq. (8) we get

$$\hat{c} = \frac{1}{N(N-1)} \sum_{i \neq j} \int_{\Omega} \mathcal{K}^{c}(\boldsymbol{u}) \delta\left(\boldsymbol{u} - \boldsymbol{x}_j + \boldsymbol{x}_i\right) \mathrm{d}\boldsymbol{u} \tag{B.2}$$

$$= \frac{1}{N(N-1)} \sum_{i \neq j} \mathcal{K}^{c}\left(\boldsymbol{x}_j - \boldsymbol{x}_i\right) , \tag{B.3}$$

which can be used to measure the crowding index in the population, given a spatial distribution of organisms and for a known competition kernel.

Similarly, we apply the same procedure to compute the crowding index using the spatial pattern of home-range centers and space utilization functions. We first compute the home range competition kernel $\mathcal{K}^{\mathrm{HR}}(\boldsymbol{u})$. Since the asymptotic displacement from the home-range center of the organisms following OU movement and the competition kernel $\mathcal{K}^{c}$ we implemented are Gaussian distributions centered at zero, their convolution is also a Gaussian distribution centered at zero. The crowding index based on home-range centers can then be computed as

$$\hat{c} = \frac{1}{N(N-1)} \sum_{i \neq j} \mathcal{K}^{\mathrm{HR}}\left(\bar{\boldsymbol{x}}_j - \bar{\boldsymbol{x}}_i\right) , \tag{B.4}$$

where $\bar{\boldsymbol{x}}_i$ denotes the position of the home range center of the i-th organism.

C Supplementary Figures

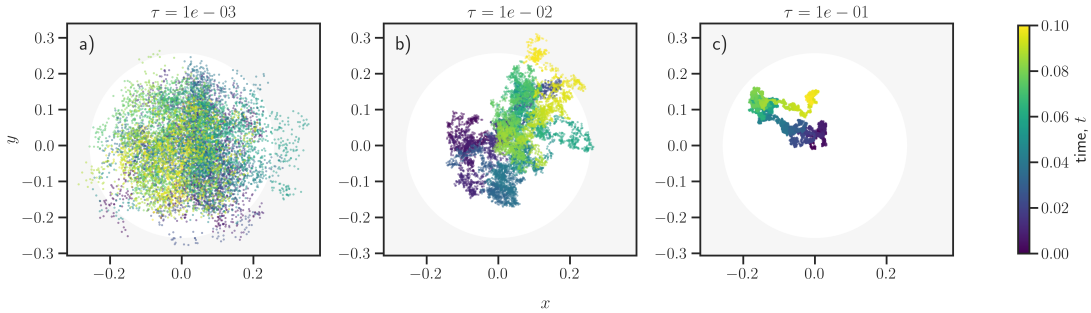

Figure C.1: The effect of home range crossing time on how fast OU-moving individuals cover their entire home range. Organisms take longer to explore their entire home range when the home-range crossing time τ increases (from panel a to c), keeping home-range size fixed, $A_{\mathrm{HR}} = 0.20(a.u.)$. In the three panels, we simulated a single trajectory for a total of $t = 0.1(a.u.)$ with time increments of $dt = 10^{-5}(a.u.)$. For smaller values of τ (panel a), the organism effectively explores the entire HR. However, if τ increases but we keep the simulation time constant, the organism explores a more restricted region of its home range. In the limit where τ tends to zero, the trajectory loses all the autocorrelation between consecutive locations, which becomes an independent and identically distributed variable (IID). Consequently, the organism can be found anywhere within the home range at each time step.

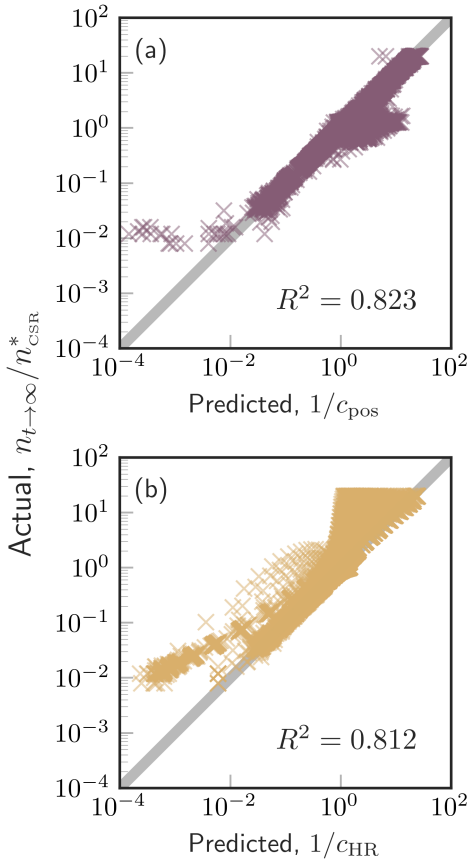

Figure C.2: Accuracy of the crowding index for broader dataset. The crowding index measured using only information about spatial scales across all the simulations matches the measurement of the carrying capacity of the population. The abundance of the population in the simulation normalized by the carrying capacity of a homogeneous population (y-axis) is compared to the inverse of the crowding coefficient (x-axis). (a) The crowding index was measured using the actual position of the organisms as the average local density experienced by each organism in a snapshot of the simulation. (b) The crowding index was measured based on the expected mortality rate an organism experiences given its home range size and the distances between its home range center and that of its neighbors. The complete agreement (1-1 line) is represented as a gray line in the background of each panel and the R^2 is reported as an indicative of the goodness of fit. No data was filtered out of the analysis, apart from simulations in which extinction was observed.